International Journal of Heat and Mass Transfer 54 (2011) 797–806

Contents lists available at ScienceDirect

International Journal of Heat and Mass Transfer

journal homepage: www.elsevier.com/locate/ijhmt

Temperature-dependent aggregation and diffusion in nanofluids

Patricia E. Gharagozloo *, Kenneth E. Goodson

Department of Mechanical Engineering, Stanford University, Stanford, CA 94305, United States

ARTICLE INFO

Article history:
Received 18 March 2010
Accepted 10 June 2010
Available online 10 November 2010

Keywords:
Nanofluid
Aggregation
Thermal diffusion
Thermal conductivity
Viscosity
Monte Carlo simulation
Nanoparticle

ABSTRACT

While particle aggregates play a central role in recent models for nanofluid thermal conductivity, the effect of particle diffusion in a temperature field on the aggregation and transport has yet to be studied in depth. The present work separates the effects of particle aggregation and diffusion using parallel plate experiments, infrared microscopy, Monte Carlo simulations, and rate equations for particle and heat transport. The predicted thermal conductivity and viscosity enhancements are compared to determine the favorability of aggregating nanofluids. Experimental data show non-uniform temporal increases in thermal conductivity and are well described through simulation of the combination of particle aggregation and diffusion. The simulation shows concentration distributions due to thermal diffusion causing variations in aggregation, thermal conductivity and viscosity. The aggregation produces an unfavorable nanofluid. An optimum nanoparticle diameter is calculated to minimize settling, thermal diffusion and aggregation.

1. Introduction

Nanofluids of metal and metal oxide nanoparticles suspended in fluids have generated much interest in applications including cancer detection and treatment [1], interface lubrication, and electronics cooling. Much attention has been on cooling applications due to reports of thermal conductivity enhancements much greater than those predicted by effective medium theory (EMT), which for dilute suspensions of well-dispersed nanoparticles with $k_p \gg k_f$ predicts a 3% increase for every 1%$_{vol}$ concentration. The high thermal conductivities reported could allow for large improvements in current fluidic system cooling abilities. Past work proposed hypotheses to explain the thermal conductivity enhancement including Brownian motion induced micro-convection [2–6], near field radiation [7], and liquid layering [8–10], which have been questioned by multiple researchers [11–13].

Effects of aggregation are found in the nanofluid studies by various research groups, but are often unaccounted for. Past measurements of viscosity showed increases of 10% or higher per 1%$_{vol}$ concentration [14–19]. This exceeds the predictions of Einstein in 1911 [20,21] for well dispersed nanoparticle suspensions of 2.5% per 1%$_{vol}$ concentration. Optical thermal conductivity measurements using forced Rayleigh scattering [22] and beam deflection [23] techniques yielded data consistent with EMT. Researchers that noted aggregation or opaque fluids with aggregates large enough to scatter light measured higher thermal conductivities than predicted by EMT [24–27]. Aggregation models account for the increases in thermal conductivity and viscosity. For microchannel heat exchangers, it is particularly important to understand the correlation between the enhancement in thermal conductivity and viscosity. A recent benchmark study consisting of 34 research groups has shown that for a variety of stable, well-dispersed nanofluids, the thermal conductivity is well modeled through the Maxwell Effective Medium Theory [28]. Thus, aggregation is an important factor for thermal applications of any nanofluid.

Several groups have studied the time evolution of the nanofluid thermal conductivity finding significant initial enhancements in the thermal conductivity that decrease substantially over time. The particle sizes for these studies were typically 10 nm or less, while the aggregate sizes were found to become >1 μm. In the worst cases, a significant amount of settling was noticed [29–32]. Gharagozloo et al. [33] found with a stabilized nanofluid the thermal conductivity increased over time. Aggregation and settling are two mechanisms behind the time evolution of the thermal conductivity. As the aggregates become large (>1 μm) settling occurs causing a decrease in particle concentration and thermal conductivity. Potentially large enhancements can occur in stabilized solutions if aggregates are less dense and small enough to stay in solution.

The effect of aggregation on thermal conductivity has been modeled by a few research groups. Calculations for typical aggregates give potential enhancements of 5% per 1%$_{vol}$ concentration for dense aggregates and up to 30% for sparse aggregates [11,34–39]. Gharagozloo and Goodson [40] measured aggregate fractal dimensions over time for alumina nanofluids and showed increased aggregation with increasing concentration and temperature in isothermal

* Corresponding author. Address: 7011 East Ave, Livermore, CA 94551, United States. Tel.: +1 925 294 2122; fax: +1 925 294 3870.
E-mail address: peghara@sandia.gov (P.E. Gharagozloo).

0017-9310/$ - see front matter © 2010 Elsevier Ltd. All rights reserved.
doi:10.1016/j.ijheatmasstransfer.2010.06.058

Nomenclature

A	area
c	particle concentration
d	diameter
D	diffusion coefficient
D_T	thermal diffusivity
d_f	fractal dimension
d_l	chemical dimension
j	particle flux
k	thermal conductivity
N	number of particles
q	heat flux
r	radius
R	radius of gyration
S_T	Soret coefficient
T	time

Greek symbols

α	enhancement factor
φ	volume fraction
μ	viscosity

Subscripts

agg	aggregate
c	percolation contributing
eff	effective
f	fluid
nc	non-percolation contributing
p	particle

conditions. Philip et al. [41] measured the linear aggregation of stabilized magnetite particles in a magnetic field and measured an enhancement of 64%. Diffusion has been shown to strongly influence the local particle concentration and thus aggregation, thermal conductivity, and viscosity in flow channels [42–44]. To fully understand the potential of aggregated nanofluids a study of aggregation in a temperature gradient situation is necessary.

The present work isolates the effects of aggregation and thermal diffusion on the nanofluid thermal conductivity. Experimental data obtained using high resolution infrared microscopy are compared to a Brownian motion base Monte Carlo simulation of nanofluids subjected to a temperature field utilizing the models for fluid properties from the previous studies. A numerical simulation of the thermal diffusion is compared to the Monte Carlo results without aggregation to verify the results and estimate the Soret coefficient. Results show the combined effects of aggregation and thermal diffusion on the thermal conductivity distribution. Predicted values of thermal conductivity and viscosity are compared to determine the effectiveness of nanofluids over the base fluid.

2. Experimental apparatus

2.1. Full field infrared imaging

A calibrated high-resolution infrared microscope (QFI/Infrascope) measures the full-field temperature distribution. Fig. 1 shows a schematic of the experimental setup. The IR focal plane array uses an array of InSb elements (256×256) with detection wavelengths of 2–5.5 μm and 0.1 K temperature sensitivity. A 15x SiGe objective with numerical aperture of 1.0 provides spatial resolution of 2.8 μm. Two 1 in., square, copper plates spaced 500 μm apart by glass spacers hold the nanofluid. The average Rayleigh number of the system with water is 160, which is much less than the limit of 1000 for buoyancy-driven flow to stay weak and heat transfer to be primarily through conduction. A 250 μm thick Kapton heater (Omega/KHLV-101) generates joule heat that conducts across the nanofluid and dissipates into a temperature controlling thermoelectric cooler and water cooled heat sink. The heat flux sensor (Omega/HFS-3) monitors any variations from the applied power. An humidification chamber reduces evaporation.

A 20 μm thick polyester film covers the fluidic opening, serves as a uniform emissivity emitter, precisely defines the emission location, and reduces fluidic evaporation. The heat traveling through the film is calculated using a thermal resistor network as less than 0.06% of the applied heat. A COMSOL finite element thermal model predicts the difference in the calculated thermal conductivity from the temperature of the film compared to the fluid temperature to be less than 3%. To obtain the thermal conductivity, 256 temperature distribution lines are averaged and the gradient calculated.

The emissivity is calibrated for each measurement by a two temperature surface emissivity correction at temperatures characteristic of the measurement. The calibration is applied to the measurement images and corrects for reflected signal components and emissivity spatial and temperature dependencies. Heat loss from the experimental apparatus to the environment is due to natural convection from the outer surfaces, conduction through the back insulator, and minor fluid evaporation. These losses are found to be less than 5% of the applied heating power and are systematically eliminated as part of the data extraction procedure. The ability to precisely determine the temperature-dependent conductivity of pure water is verified before each measurement. The thermal conductivities are found to have repeatability to within 5% of the average value.

2.2. Nanofluid preparation

The nanofluid studied in the present work is the same as that studied by Gharagozloo and Goodson [40]. The nanofluid has 20% weight concentration alumina in H_2O with less than 1% nitric acid

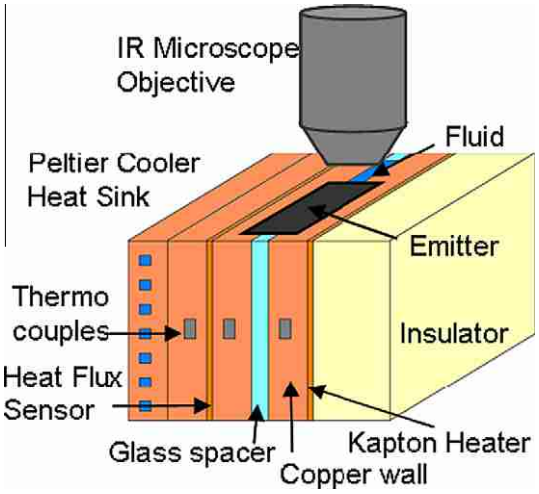

Fig. 1. Schematic of infrared microscope experimental setup showing nanofluid held between copper plates and glass spacers. A heat flux is applied across the nanofluid with a thin Kapton heater, measured on the opposite side with a heat flux sensor, and dissipated into a thermoelectric cooler and heat sink. The temperature is monitored with thermocouples on the copper plates.

(Alfa Aesar/12733). The fluid is diluted with deionized water to the desired volume concentrations. Prior to the measurements the nanofluid is sonicated (Fisher Scientific/FS30) continuously for 4 h at 60 Hz and 130 W. The nanofluid is stable with only minor settling after a week at room temperature. The pH of each of the nanofluids is measured using pH test strips (Indigo Instruments/3381) with a pH range of 1–14. The pH values are read with an accuracy of ±0.5. The measured pH for each of the nanofluid concentrations is 5.5 and for the deionized water is 6. DLS measurements performed on a solution diluted to $0.05\%_{vol}$ concentration yield a nominal particle diameter of 40.2 nm, a relative variance of 0.02, and skew in the decay of 11.5 nm towards larger diameters. A small number of sintered particles, less than 0.5%, are initially present with a nominal diameter of 125 nm. These sintered aggregates are large enough to scatter visible light and reduce the transparency of the nanofluid.

3. Monte Carlo simulation methodology

Methods of modeling particle aggregation vary depending on the desired output. The Monte Carlo method allows for direct simulation of the system. Two main types of Monte Carlo simulation of aggregation are typically used. The first allows for the simulation of the growth and structure of the aggregates [45,46]. The second allows for extraction of bulk effects due to the aggregation. Spielman and Levenspiel [47] showed the effectiveness of a Monte Carlo simulation for a system of reacting, coalescing droplets by randomly choosing two droplets to coalesce, mix and redistribute at a constant rate. Shah et al. [48] expanded the simulation procedure by modeling the random behavior in terms of probability functions and advancing time based on the expected time for the event to occur. Liffman [49] calculated the probability of one cluster/particles interacting with another. Based on the probability a single particle was randomly chosen to interact and another particle was randomly chosen to interact with it. From the simulation, they modeled the size distribution of the clusters over time. Kruis et al. [50] proposed a simpler version by summing the collision functions for each possible particle pairs and choosing pairs to aggregate based on a comparison between a random number and the relative magnitude of a pairs collision function. After each iteration, the time is progressed based on the number of aggregating pairs. For both of these last simulations no regard is given to the position of the particles in the system.

3.1. Particle initialization and aggregation

In this study, the method of Kruis et al. [50] is expanded on to determine the aggregate size variation across the temperature gradient and calculate the variation of the properties [51]. Rather than allow aggregation between any particles in the simulated system, only pairs near each other are considered as potential aggregates. Instead of choosing a time step based on the number of aggregating pairs, the number of aggregating pairs is chosen from the time step. The simulation determines the time evolution of the concentration distribution and aggregate sizes. The particles are initially uniformly distributed within the modeled area. At each time step, a normally distributed random displacement is applied to each particle in the x and y directions with mean zero and variance $2D\Delta t$. The simulation accounts for the temperature dependence of the viscosity and diffusion coefficient and applies specular reflection at the boundaries.

Aggregation is a process in which initially dispersed particles join together [52]. The aggregate size increases with time as more particles join. In colloids, particles are dispersed in fluid and diffuse under Brownian motion. The particles act independently until they come close enough to experience Van der Waals forces and stick together. Particles may ricochet off each other multiple times due to the electrostatic barrier before actually joining into an aggregate. To model these effects efficiently, the aggregation is modeled through a three step process. The expected number of aggregating collisions in a given time step is calculated from the inverse of the sum of the collision frequency function, β, for all particle pairs. For Brownian limited aggregation the collision frequency function derived from Fick's law is given by [50,53,54]:

$$\beta_{ij} = 4\pi(D_i + D_j)\cdot(r_i + r_j) \tag{1}$$

Pairs of particles separated by less than their average diameter are identified as potentially aggregating collisions. Potentially aggregating collisions are chosen randomly to aggregate up to the expected number of aggregating collisions. The time step is sufficiently small to ensure more potentially aggregating collisions are identified than the number of expected aggregating collisions.

The simulation keeps track of the number of particles in, the average diameter of the particles in, the predicted radius of gyration of, and the hydraulic diameter of the aggregates. The radius of gyration is calculated by equating the particle volume fraction within the aggregate from two formulas, the first based on volume fraction (Eq. (2)), the second from 3D fractal theory of aggregates (Eq. (3)):

$$A_{agg} = \frac{NA_p}{\varphi_{p,agg}} = \pi R_a^2 = \frac{N\pi d_p^2}{2^2\varphi_{p,agg}} \rightarrow \varphi_{p,agg} = \frac{Nd_p^2}{4R_a^2} \tag{2}$$

$$\varphi_{p,agg} = \left(\frac{2R_a}{d_p}\right)^{d_f-3} \tag{3}$$

where $\varphi_{p,agg}$ is the particle volume fraction in the aggregate, N is the number of particles in the aggregate, d_p is the average particle size in the aggregate, R_a is the radius of gyration of the aggregate, and d_f is the fractal dimension of the aggregate. We assume the aggregates are sparse enough, given their low fractal dimension, for the two dimensional area concentrations to equal the three dimensional volume concentrations. The fractal dimension is a measure of the change in particle density with distance from the center of the aggregate and typically varies between 1.7 and 2.5 for 3D. It relates the particle volume fraction in the aggregate to the aggregate radius of gyration through the power law given in Eq. (3). Using areas in the formulation is necessary due to the 2D model, which results in a potential error of a factor of 4/3 when equating Eqs. (2) and (3).

3.2. Effective thermal conductivity

The thermal conductivity of the aggregates is calculated by separating them into two components, the percolation contributing backbone and non-percolation contributing dead-ends [39]. The effective thermal conductivity of the dead-end particles, k_{nc}, is calculated using the Bruggeman model, which is appropriate for high particle volume fractions [55]:

$$\sum_i \frac{\varphi_i(k_i - k_{nc})}{k_i + 2k_{nc}} = 0 \tag{4}$$

where φ_i is the volume fraction of the non-percolation contributing aggregate components (fluid and dead-end particles) and k_i is the thermal conductivity of the components. The effective thermal conductivity of the aggregate, k_{agg}, is calculated using composite theory for completely misoriented ellipsoidal particles, for the backbone, in a matrix of the non-percolation contributing portion. The following equations are used [56]:

$$k_{agg} = k_{nc}\frac{3+\varphi_c(2\beta_{11}^c(1-L_{11})+\beta_{33}^c(1-L_{33}))}{3-\varphi_c(2\beta_{11}^c L_{11}+\beta_{33}^c L_{33})} \tag{5}$$

$$L_{11} = \begin{cases} 0.5p^2/(p^2-1) - 0.5p\cosh^{-1}p/(p^2-1)^{1.5} & p>0 \\ 1/3 & p=0 \end{cases} \tag{6}$$

$$L_{33} = 1 - 2L_{11} \tag{7}$$

$$\beta_{ii}^c = (k_{ii}^c - k_{nc})/(k_{nc} + L_{ii}(k_{ii}^c - k_{nc})) \quad i = 1,3 \tag{8}$$

$$k_{ii}^c = \frac{k_p}{(1+\gamma L_{ii}k_p/k_f)}, \left(\text{with } \gamma = \left(2+\frac{1}{p}\right)\alpha,\ \alpha = \frac{2R_b k_f}{d_p}\right) \tag{9}$$

where R_b is the boundary resistance between the particle and the fluid and p is the ratio between the length of the percolating chain to the particle size. The effective thermal conductivity of the nanofluid is found through the Maxwell effective medium theory [57] for dispersed particles and is given by:

$$k_{eff} = k_f\frac{k_{agg}+(n-1)k_f-(n-1)\varphi_{agg}(k_f-k_{agg})}{k_{agg}+(n-1)k_f+\varphi_{agg}(k_f-k_{agg})} \tag{10}$$

where φ_{agg} is the volume fraction of aggregates in the fluid and $n = 3/\psi$ where ψ is the sphericity of the aggregate. A spherical aggregate is assumed yielding $n = 3$.

The volume fraction of the particles in the aggregate is given by Eq. (3) and $\varphi_{p,agg} = \varphi/\varphi_{agg}$ and the volume fraction of the backbone particles in the aggregate is $\varphi_c = (2R_a/d_p)^{d_l-3}$, where d_l is the chemical dimension of the aggregates. The chemical dimension is a measure of the branch dimensions within the aggregate and theoretically varies between 1 and d_f though a maximum value of 1.6 is imposed by the self-avoiding random walk [58]. It relates the concentration of backbone particles within the aggregate to the radius of gyration of the aggregate through a power law. The volume fraction of dead-end particles in the aggregate is $\varphi_{nc} = \varphi_{p,agg} - \varphi_c$. A limit is imposed on the size of the aggregates based on the fractal theory by setting $\varphi_{agg} = 1$ yielding a maximum radius of gyration of $R_{a,max} = (d_p/2)\varphi^{1/(d_f-3)}$.

To estimate the effect of aggregation and thermal diffusion on the viscosity and the viscosity profile, the bulk effective viscosity of the nanofluid is calculated. The effective hydrodynamic viscosity for a fluid containing fractal aggregates is modeled by [58]:

$$\mu_{eff} = \mu_f\left(1-\frac{\varphi_{agg}}{\varphi_{max}}\right)^{-2.5\varphi_{max}} \tag{11}$$

where $\varphi_{max} = 0.61$ is the maximum possible volume concentration in the aggregate for rigid spheres. This equation is most appropriate for higher shear rates, where most nanofluids have been found to have less shear thinning [14].

The Monte Carlo simulation allows for the modeling of aggregation and thermal diffusion based on local concentrations and temperatures. For this simulation, aggregation is assumed to be diffusion limited, aggregates are assumed to be spherical, and the fractal dimension is assumed to be less than 2. No surface effects are accounted for in the simulation. The thermal conductivities of the aggregates are calculated using composite theory assuming no interfacial resistance between the particles due to ballistic transport.

4. Diffusion simulations

A numerical simulation models the thermal diffusion for non-interacting particles in the experimental setup. The concentration and temperature profile over time is modeled through a numerical simulation of the appropriate Onsager relation [59] for the particle and heat flux given below:

$$j = -D\nabla c - D_T c\nabla T \tag{12}$$

$$q = -c_1\nabla T - c_2\nabla c \tag{13}$$

where j is the particle flux, D is the diffusion coefficient, T is the temperature, c is the particle number concentration, $D_T = S_T D$ is the thermal diffusivity, q is the heat flux, and c_1 and c_2 are unknown coefficients. The Soret coefficient, S_T, is used as a fitting parameter to compare the numerical model to the Monte Carlo simulation without aggregation. Previous work showed $c_2\nabla c$, which represents the Dufour effect [59], is multiple orders of magnitude smaller than $c_1\nabla T$ and is negligible [31]. Thus, c_1 is the thermal conductivity k_{eff}. The coupled differential equations for the particle and heat flux are discritized with the control volume technique.

The diffusion coefficient is modeled using Stoke's drag for a spherical particle and is given by:

$$D = \frac{k_b T}{3\pi\mu_f(T)d_p} \tag{14}$$

where k_b is the Boltzmann constant, μ_f is the temperature dependent base fluid viscosity, and d_p is the particle diameter.

The temperature is calculated at each time step using the effective thermal conductivity of each element and the second Onsager equation, which reduces to Fourier's law $dT/dx = -q/k_{eff}$. The effective thermal conductivity is calculated using Maxell's effective medium theory taking into account the variation in concentration across the temperature field due to the thermal diffusion.

To solve for the time evolution of the concentration distribution, the divergence of the first Onsager equation is taken yielding:

$$\frac{\partial c}{\partial t} = \nabla\cdot(D\nabla c) + \nabla\cdot(DS_T c\nabla T) \tag{15}$$

The change in the concentration for each element at a particular time step is calculated from the fluid properties and the local concentration and temperature gradients.

To summarize, the flux and resulting concentration gradient of non-interacting particles in a temperature gradient is modeled through the appropriate Onsager relation. We assume the Dufour effect is negligible, which results in no additional heat flux due to the concentration gradient.

5. Results and discussion

For the Monte Carlo simulation the particle sizes are distributed based on the DLS measurements of the nanofluid with nominal particle sizes of 40, 60, 80, and 130 nm. Concentrations of 1%, 3%, and 5%$_{vol}$ are used. The temperature of the cold boundary is held at 20 °C and a heat flux of 4 W/cm^2 is applied at the opposite boundary as in the experiments for both simulations. For the Monte Carlo simulation, d_f is taken as 1.8, which is the measured average measured fractal dimension for these aggregate formations using static light scattering [40] and d_l is taken as 1.0, 1.4, and 1.6 where the value of 1.4 corresponds to the typical value found for suspensions [57].

5.1. Comparison of Monte Carlo without aggregation and numerical model

The steady state solution from the Monte Carlo model without aggregation and the numerical model are fitted using S_T as the fitting parameter. From this comparison, the effective Soret coefficient in the fluid is estimated to be 0.025 K^{-1}, which compares to estimated maximum values of 0.01 and 0.1 K^{-1} for C_{60}–C_{70} fullerenes and 4 nm gold particles, respectively [44,60]. The concentration profile from the Monte Carlo simulation and the numerical model with this Soret coefficient are plotted in Fig. 2 at multiple times showing good agreement in both the magnitude and shape of the curves. From Maxwell's effective medium theory, the variation in concentration would result in the expected enhancement to

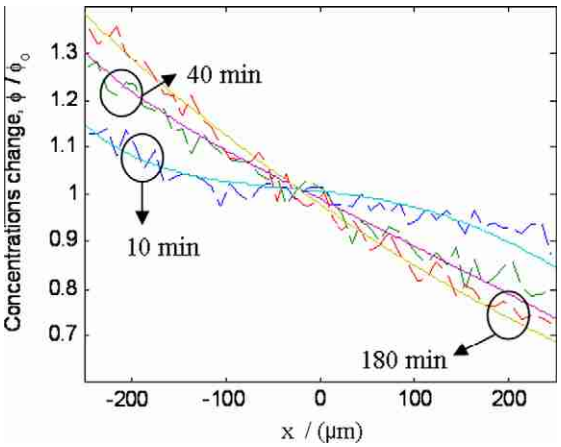

Fig. 2. Predictions of normalized particle distribution across the channel for Monte Carlo simulation without aggregation or particle interaction (dashed) and numerical model (solid) for a S_T of 0.025 K^{-1} and d of 40 nm at times of 10, 40 and 180 min for alumina nanoparticles in water subjected to a heat flux of 4 W/cm^2.

increase 4% at the cold boundary and decrease 4% at the hot boundary.

5.2. Monte Carlo results for particle concentration effect

The distribution of the average radius of gyration of the aggregates across the nanofluid for the three concentrations is shown for various times in Fig. 3. The aggregates in the higher concentrations and cold regions grow faster. It is expected [40] that the aggregates will grow faster in high temperatures; however, due to the increased concentration at the lower temperatures this is not observed. The predicted distribution of the increase in nanofluid thermal conductivity from the Monte Carlo simulation for each concentration at various times is shown in Fig. 4. The time evolution of the thermal conductivity for the 1%$_{vol}$ concentration is very small. When taken to 130 simulated minutes, the simulation begins to show a rise in the thermal conductivity in the cold region. For the 3% and 5%$_{vol}$ concentrations, the increases in thermal conductivity begin to occur early and become large after an hour of simulated time. The cold region experiences much larger increases in the thermal conductivity than the hot region in both concentrations due to the diffusion of particles to the cold region combined with the increase in aggregation due to the higher concentrations. These results correspond with the higher concentrations and larger aggregate sizes present in the cold region compared to the hot region.

The inclusion of a typical boundary resistance between alumina and water of 0.77×10^{-8} K m^2/W lowers the average effective thermal conductivity by less than 5%. A comparison for the average effective thermal conductivity with and without a boundary resistance is plotted in Fig. 5. The chemical dimension is varied between 1 and 1.6 and the resulting thermal conductivity is plotted in Fig. 6. There is little variation at early time with less aggregation. A variation of 5% between 1 and 1.6 cases occurs after two hours of simulated time.

5.3. Monte Carlo results for the effective viscosity

The ratio of the calculated viscosity enhancement factor, $\alpha_{visc} \equiv (\mu_{eff}/\mu_f - 1)/\varphi$ and thermal conductivity enhancement factor, $\alpha_{cond} \equiv (k_{eff}/k_f - 1)/\varphi$ for the three volume concentrations is plotted in Fig. 7. Through thermal and hydraulic analysis for laminar flow in a circular tube, Prasher et al. [14] showed that this ratio should be less than 4 for nanofluids to be more favorable than the base fluid for microchannel heat exchangers. This is considered a best case scenario heat exchanger design, where as a worst case scenario would require the thermal conductivity enhancement to be greater or equal to the viscosity enhancement. For lower amounts of aggregation, the ratio stays favorable. At longer times and higher concentrations the nanofluid becomes unfavorable.

The predicted viscosity distribution from the Monte Carlo simulation for the 3%$_{vol}$ concentration is shown in Fig. 8. The viscosity in the cold region doubles after an hour, while the viscosity in the hot region shows little change. For this set up, the expected increase in the viscosity from the hot region to the cold region is a factor of 1.7. In laminar flow it has been shown [57] that the fractal dimension of the aggregates is reduced from 1.8 to 2.3 due to the shear forces, which reduces the effective viscosity. The shear effects of the flow will also cause greater concentration and viscosity distributions as particles are forced towards the center of the channel cross-section away from the channel walls. In turbulent flows, aggregates may be broken up and the favorability criteria may differ from the current analysis.

5.4. Experimental results for thermal conductivity

The thermal conductivity is calculated using Fourier's Law for heat diffusion, $q'' = -k\nabla T$, where ∇T is the slope of the ensemble averaged temperature distribution and q'' is the estimated actual heat flux. The total temperature difference across the cavity is

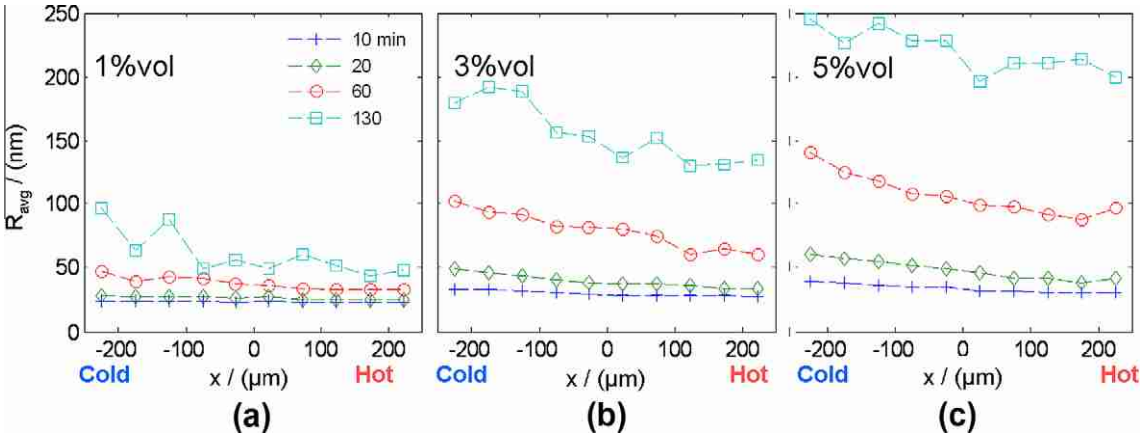

Fig. 3. Predictions of average aggregate radius of gyration distribution across the nanofluid at various times from the Monte Carlo simulation for (a) 1%, (b) 3%, and (c) 5%$_{vol}$ concentrations of nominal diameter alumina nanoparticles in water subjected to a heat flux of 4 W/cm^2.

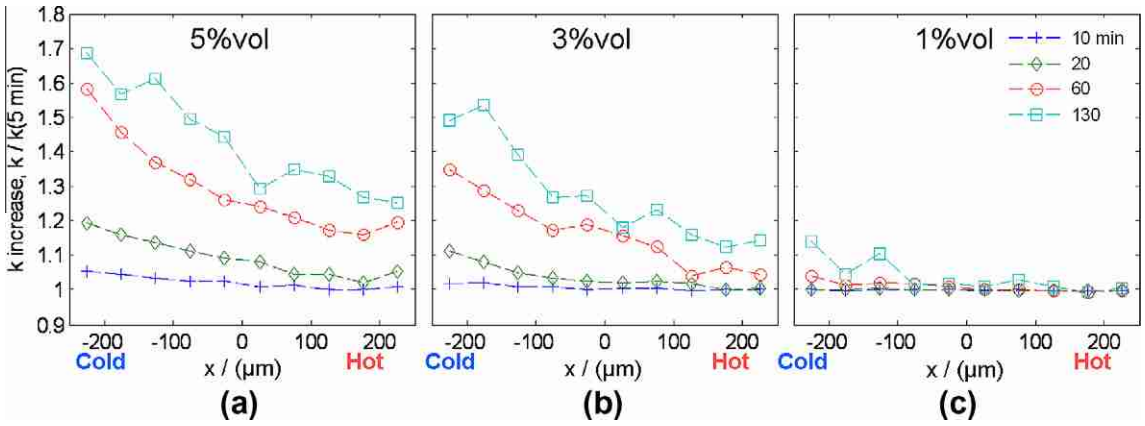

Fig. 4. Predictions of thermal conductivity distribution across the nanofluid at various times from the Monte Carlo simulation for (a) 5%, (b) 3% and (c) 1%$_{vol}$ concentrations of 40 nm nominal diameter alumina nanoparticles in water subjected to a heat flux of 4 W/cm^2.

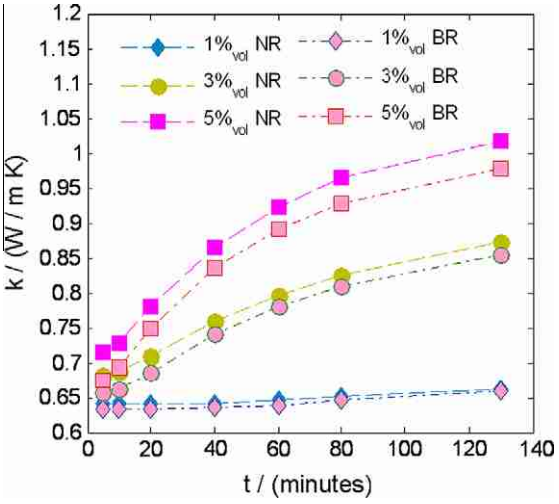

Fig. 5. Plot of the predicted average thermal conductivity over time from the Monte Carlo simulation with no boundary resistance (dashed) and with typical boundary resistance of 0.77 m^{2}K/W between alumina and water (dash-dot).

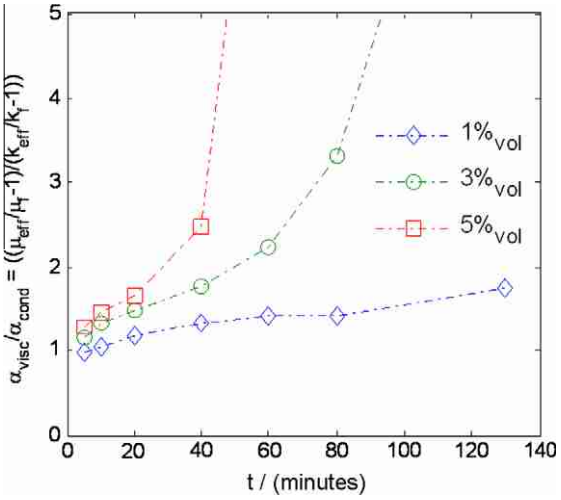

Fig. 7. Predictions of ratio of the average viscosity and thermal conductivity enhancement over time from the Monte Carlo simulation for 1%, 3%, 5%$_{vol}$ concentrations and 40 nm particle diameter.

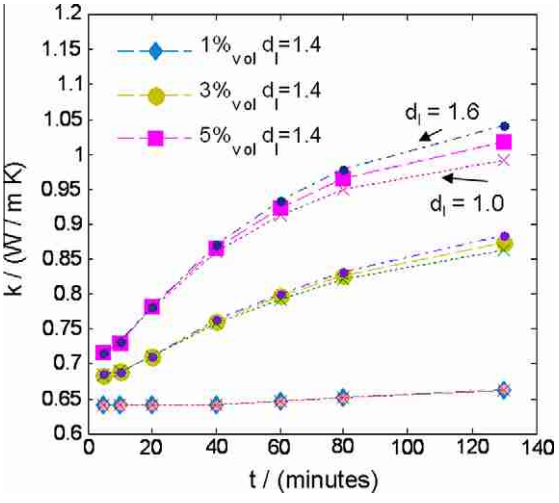

Fig. 6. Plot of the predicted average thermal conductivities over time from the Monte Carlo simulation for the 1%, 3% and 5%$_{vol}$ concentrations for d_l = 1 (dot/×), 1.4 (dash) and 1.6 (dash-dot/·).

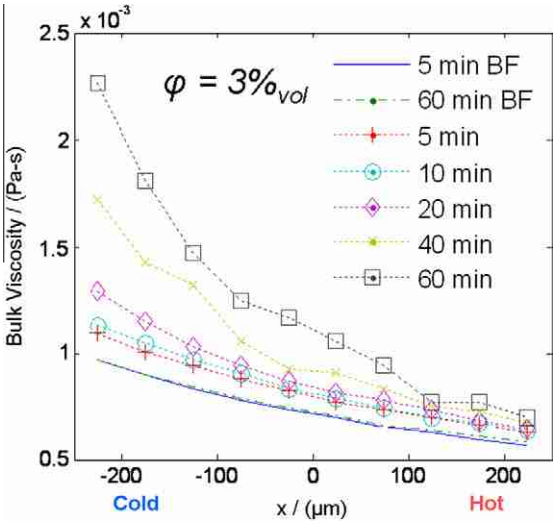

Fig. 8. Predictions of viscosity distribution of the base fluid and nanofluid across the channel at various times from the Monte Carlo simulation for 3%$_{vol}$ concentrations of 40 nm nominal diameter alumina nanoparticles in water subjected to a heat flux of 4 W/cm^2.

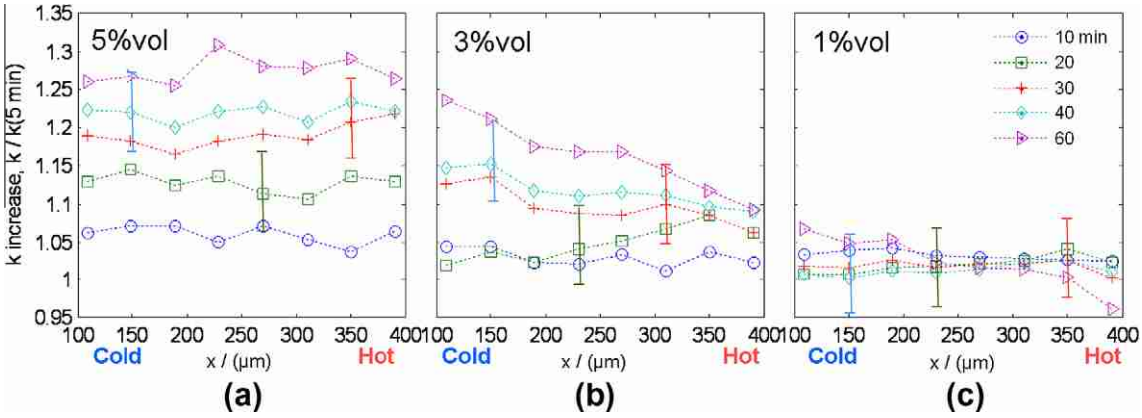

Fig. 9. Experimentally measured thermal conductivity distribution data across the nanofluid at various times for (a) 5%, (b) 3% and (c) 1%$_{vol}$ concentrations of 40 nm nominal diameter alumina nanoparticles in water subjected to a heat flux of 4 W/cm^2.

25 °C with 25 W of heating and a mean temperature of 50 °C. Emitter film curvature at the edge of the copper plates prevents the evaluation of the outer 70 μm of the image. The thermal conductivity profile is evaluated by calculating the slope of nine 40 μm temperature divisions with 50% overlap. Fig. 9 shows the measured distribution of the nanofluid thermal conductivity increase for each concentration at various times. Small droplets condensing on the emitting film during the measurement create slight waviness in the plots which slightly skew the calculations. The 1%$_{vol}$ concentration yields no discernable changes in conductivity over time considering the experimental uncertainty. The 5%$_{vol}$ concentration yields a spatially uniform increase in thermal conductivity over time. The 3%$_{vol}$ concentration yields an increase in thermal conductivity over time with a larger increase in the cold region of the fluid.

5.5. Comparison of Monte Carlo and experimental results for thermal conductivity

The average thermal conductivity from the Monte Carlo simulation and the experimental measurement for each concentration is shown in Fig. 10. For each volume concentration, the initial experimental thermal conductivity value starts at close to the effective medium theory. The simulation and the experiment show good agreement in both magnitude and curvature. Both show the thermal conductivity increase flattening over time as the aggregation progresses. The experimental data appears to be shifted in time to the left. This is likely due to the nanofluid sitting for about 15 min after sonication while the IR system is calibrated to the new surface emissivity, which would allow aggregation to occur before the measurement begins.

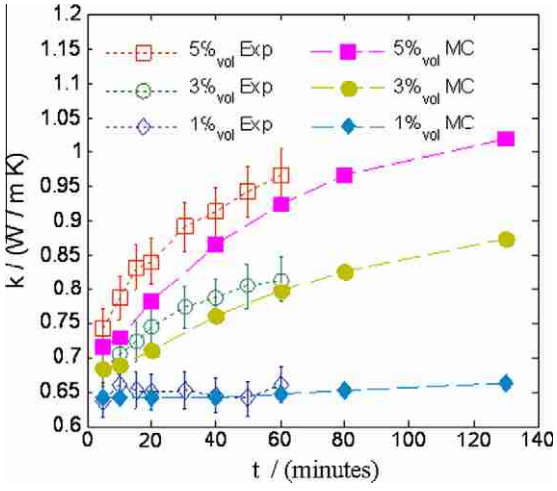

Fig. 10. Plots of the average thermal conductivity of the nanofluid over time predicted from the Monte Carlo simulation (dashed/solid) and experimentally measured data (dotted/hollow) for 1%, 3%, and 5%$_{vol}$ concentrations of 40 nm nominal diameter alumina nanoparticles in water.

In both the simulation and experimental measurement the variations in the distribution of the nanofluid thermal conductivity increase for the 1%$_{vol}$ concentration are small. For the 3%$_{vol}$ concentration both the simulation and experiment show larger increases in the cold region than in the hot region. The simulation predicts more of a variation across the nanofluid than measured. For the 5%$_{vol}$ concentration the experiment shows a constant increase across the whole nanofluid while the simulation shows larger increases in the cold region. These differences between the simulation and experiment for the 3% and 5%$_{vol}$ concentrations are likely due to the time period between sonication and the measurement during the system calibration. The aggregate growth during this time period slows the diffusion reducing the concentration distribution.

5.6. Monte Carlo results for initial particle size effect

Fig. 11 plots the average radius of gyration of the aggregates over time predicted by the Monte Carlo simulation for 5%$_{vol}$ concentration and initial particle diameters of 40 nm, 60 nm, 80 nm, and 130 nm. As the initial particle size increases the amount of aggregation decreases due to the reduced motion and fewer particles at the same volume concentration. Fig. 12 plots the ratio of the predicted viscosity and thermal conductivity enhancement factors calculated from the Monte Carlo simulation for 5%$_{vol}$ concentration and the four initial particle diameters. Due to the reduced aggregation with the larger initial particles, the nanofluid stays favorable for the 60 nm, 80 nm, and 130 nm initial particles sizes for the simulated time period.

5.7. Particle size optimization

Variations of aggregation, diffusion and settling with initial particle size lead to the possibility of an optimum value. To estimate an optimum initial particle size, the dependence of the aggregation, diffusion and settling time constants are calculated and compared. The aggregation time constant represents the time for the total number of particles and aggregates to reduce by fifty percent and is given through slow aggregation theory [61,62] by:

$$t_p = \frac{\pi \mu_f r_p W}{k_b T \varphi_p}$$

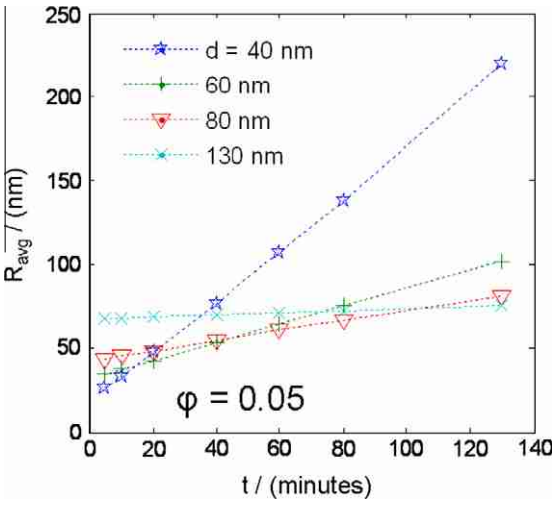

Fig. 11. Plot of the predicted average radius of gyration of the aggregates over time from the Monte Carlo simulation for 5%$_{vol}$ concentration for particle diameters of 40 nm, 60 nm, 80 nm, and 130 nm.

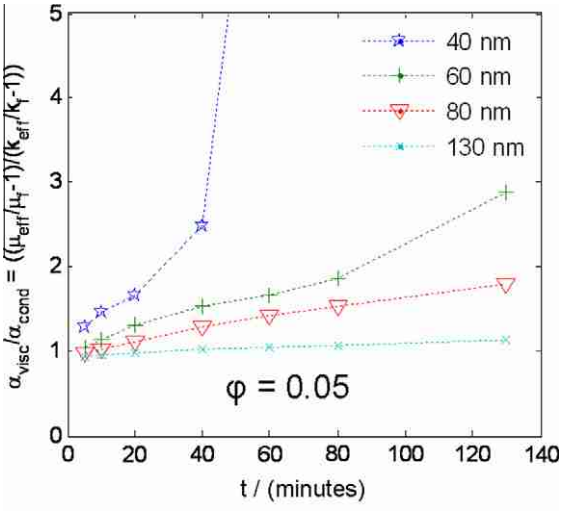

Fig. 12. Ratio of the predicted average viscosity and thermal conductivity enhancement factor over time from the Monte Carlo simulation for 5%$_{vol}$ concentration and 40 nm, 60 nm, 80 nm, and 130 nm nominal diameter.

where W is the stability ratio [63] given by:

$$W = 2r_p \int_0^\infty \frac{B(h)}{(h+2r_p)^2} \exp\left(\frac{V_T}{k_bT}\right) dh$$

where $B(h)$ is given by [64]:

$$B(h) = \frac{6(h/r_p)^2 + 13(h/r_p) + 2}{6(h/r_p)^2 + 4(h/r_p)}$$

h is the distance between the surfaces of the particles and $V_T = V_A + V_R$ is the total potential energy of interaction. V_A is the energy of attraction due to Van der Waals forces and is given by [65]:

$$V_A = -\frac{A}{6}\left(\frac{2}{s^2-4} + \frac{2}{s^2} + \ln\frac{s^2-4}{s^2}\right)$$

where $s = 2 + h/r_p$. V_R is the electrostatic energy of repulsion due to the electric double layer, which for small values of $\tau = \kappa r_p$ can be approximated by [66]:

$$V_R = \frac{\varepsilon_r \varepsilon_0 \zeta^2 r_p}{s} \exp(-\kappa h)$$

where $\kappa^2 = 2e^2 N_A I/(k_b T \varepsilon_r \varepsilon_0)$ is the Debye parameter [66], e is the elementary charge, N_A is Avogadro's number, ε_r is the relative dielectric constant of the liquid, ε_0 is the dielectric constant of free space, ζ is the zeta-potential of the particles, I is the concentration of ions in the water which is estimated by the pH [35] as 10^{-pH} for pH $\leqslant 7$ and $10^{-(14\text{-pH})}$ for pH > 7. To model the fluid of this study a temperature of 40 °C and pH of 4 is used.

The time constants for settling and thermal diffusion are calculated by equating the average distance moved by a particle undergoing Brownian motion and distance moved from the respective drift velocity:

$$\sqrt{2D\tau_d} = u_d\tau_d$$
$$\tau_d = \frac{2D}{u_d^2}$$

The drift velocity for settling is given by creeping flow over a sphere through a force balance between gravity, buoyancy, and drag given by [61]:

$$6\pi\mu_f \frac{d_p}{2} u_d = (\rho_p - \rho_f)V_p g$$
$$u_d = \frac{d_p^2(\rho_p - \rho_f)g}{18\mu}$$

where ρ is the density of the particle (p) or fluid (f), V_p is the particle volume, u_d is the drift velocity, and g is the acceleration of gravity.

The drift velocity for a particle undergoing thermal diffusion is estimated as ratio of the diffusion coefficient and the length scale, D/l, with l taken as 500 μm. The results are plotted in Fig. 13. Considering slower diffusion, settling and aggregation to be optimal, an optimum particle diameter for our system is determined by the region of intersection to be about 130 nm. This is consistent with the simulation results for diffusion and aggregation for the 130 nm particles.

6. Concluding remarks

Through experimentation and Monte Carlo simulation of aggregation and thermal diffusion, verified by a numerical model of thermal diffusion, we show that the combination of aggregation and thermal diffusion can lead to large variations in thermal con-

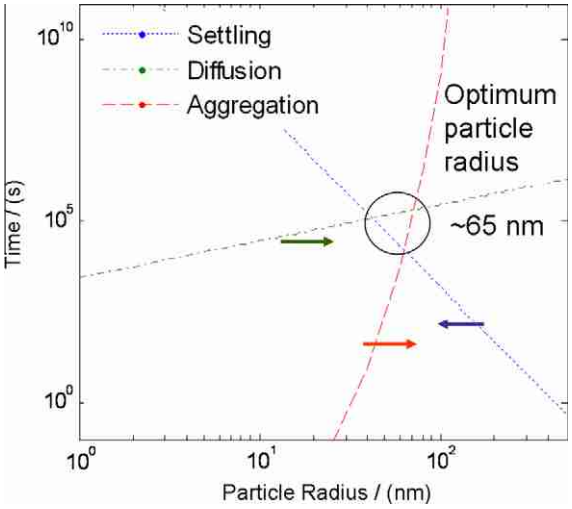

Fig. 13. Time constant for aggregation (dot), settling (dash), and diffusion (dash-dot) plotted versus particle radius. For each line the arrow points in the direction of increasing time constant and stability. The optimum particle size is found to be 130 nm.

ductivity. The aggregation of stabilized nanofluids significantly increases the thermal conductivity of the fluid. Thermodiffusion affects the amount of aggregation across a temperature gradient by creating concentration gradients causing variations in the rate of aggregation and size of aggregates within the nanofluid. Although the effects of the stabilizers are not accounted for in the simulation, it predicts the thermal conductivity of the nanofluid well through well known composite theory [55]. The expected increase in aggregation with temperature [40] is surpassed by the resulting concentration variation. Variations in the average temperature will affect the overall progression of aggregation and variations in the temperature gradient will affect the concentration gradient.

Large viscosity distributions are predicted to form due to the aggregate size distribution. As aggregation progresses the predicted viscosity increases faster than the predicted thermal conductivity causing much larger viscosity enhancement factors and unfavorable nanofluids. Increasing the particle size greatly reduces both the aggregation and thermal diffusion allowing the nanofluid to stay in the favorable regime at the higher concentrations. An optimum particle size can be determined for individual systems.

Acknowledgements

The authors acknowledge the financial support from the Office of Naval Research through Contract No. N00014-05-0374-P00001 and graduate fellowships from the National Science Foundation and Sandia National Laboratories.

References

[1] P.K. Jain, K.S. Lee, I.H. El-Sayed, M.A. El-Sayed, Calculated absorption and scattering properties of gold nanoparticles of different size, shape, and composition: applications in biological imaging and biomedicine, J. Phys. Chem. B 110 (2006) 7238–7248.
[2] S.P. Jang, S.U.S. Choi, Role of Brownian motion in the enhanced thermal conductivity of nanofluids, Appl. Phys. Lett. 84 (2004) 4316–4318.
[3] H.E. Patel, T. Sundararajan, T. Pradeep, A. Dasgupta, N. Dasgupta, S.K. Das, A micro-convection model for thermal conductivity of nanofluids, Pramana J. Phys. 65 (2005) 863–869.
[4] R.K. Shukla, V.K. Dhir, Effect of Brownian motion on thermal conductivity of nanofluids, J. Heat Transfer 130 (2008) 042406.
[5] J. Wang, G. Chen, Z. Zhang, A model of nanofluids thermal conductivity, in: Proceedings of the ASME Heat Transfer Conference, San Francisco, CA, 2005, p. 72797.
[6] J. Koo, C. Kleinstreuer, Impact analysis of nanoparticle motion mechanisms on the thermal conductivity of nanofluids, Int. Commun. Heat Mass Transfer 32 (2005) 1111–1118.
[7] P. Ben-Abdallah, Heat transfer through near-field interactions in nanofluids, Appl. Phys. Lett. 89 (2006).
[8] W. Yu, S.U.S. Choi, The role of interfacial layers in the enhanced thermal conductivity of nanofluids: a renovated Hamilton–Crosser model, J. Nanopart. Res. 6 (2004) 355–361.
[9] Q.-Z. Xue, Model for effective thermal conductivity of nanofluids, Phys. Lett. A 307 (2003) 313–317.
[10] M. Prakash, E.P. Giannelis, Mechanism of heat transport in nanofluids, J. Comput.-Aided Mater. Des. 14 (2007) 109–117.
[11] P. Keblinski, R. Prasher, J. Eapen, Thermal conductance of nanofluids: is the controversy over?, J Nanopart. Res. 10 (2008) 1089–1097.
[12] P.D. Shima, J. Philip, B. Raj, Role of microconvection induced by Brownian motion of nanoparticles in the enhanced thermal conductivity of stable nanofluids, Appl. Phys. Lett. 94 (2009) 223101.
[13] J. Eapen, W.C. Williams, J. Buongiorno, L. Hu, S. Yip, Mean-field versus microconvection effects in nanofluid thermal conduction, Phys. Rev. Lett. 99 (2007) 095901.
[14] R. Prasher, D. Song, J. Wang, P. Phelan, Measurements of nanofluid viscosity and its implications for thermal applications, Appl. Phys. Lett. 89 (2006) 133108.
[15] J.-F. Zhao, Z.-Y. Luo, M.-J. Ni, K.-F. Cen, Dependence of nanofluid viscosity on particle size and pH value, Chin. Phys. Lett. 26 (2009) 066202.
[16] W.J. Tseng, C.H. Wu, Aggregation, rheology and electrophoretic packing structure of aqueous Al_2O_3 nanoparticle suspensions, Acta Mater. 50 (2002) 3757–3766.
[17] J.-H. Lee, K.S. Hwang, S.P. Jang, B.H. Lee, J.H. Kim, S.U.S. Choi, C.J. Choi, Effective viscosities and thermal conductivities of aqueous nanofluids containing low volume concentrations of Al_2O_3 nanoparticles, Int. J. Heat Mass Transfer 51 (2008) 2651.
[18] J. Garg, B. Poudel, M. Chiesa, J.B. Gordon, J.J. Ma, J.B. Wang, Z.F. Ren, Y.T. Kang, H. Ohtani, J. Nanda, G.H. McKinley, G. Chen, Enhanced thermal conductivity and viscosity of copper nanoparticles in ethylene glycol nanofluid, J. Appl. Phys. 103 (2008) 074301.
[19] J. Lee, P.E. Gharagozloo, B. Kolade, J.K. Eaton, K.E. Goodson, Nanofluid convection in microtubes, J. Heat Transfer 132 (2010) 092401.
[20] A.J. Hughes, The Einstein relation between relative viscosity and volume concentration of suspensions of spheres, Nature 173 (1954) 1089–1090.
[21] A. Einstein, Berichtigung zu meiner Arbeit: Eine neue Bestimmung der Moleküldimensionen, Ann. Phys. 339 (1911) 591.
[22] A. Putnam, D.G. Cahill, P.V. Braun, Z. Ge, R.G. Shimmin, Thermal conductivity of nanoparticle suspensions, J. Appl. Phys. 99 (2006) 084308.
[23] D.C. Venerus, M.S. Kabadi, S. Lee, V. Perez-Luna, Study of thermal transport in nanoparticle suspensions using forced Rayleigh scattering, J. Appl. Phys. 100 (2006) 094310.
[24] J.A. Eastman, S.U.S. Choi, S. Li, L.J. Thompson, S. Lee, Enhanced thermal conductivity through the development of nanofluids, MRS Symposia Proceedings, vol. 457, Materials Research Society, Pittsburgh, 1997, p. 3.
[25] S.K. Das, N. Putra, P. Thiesen, W. Roetzel, Temperature dependence of thermal conductivity enhancement for nanofluids, J. Heat Transfer 125 (2003) 567–574.
[26] M.-S. Liu, M.C.-C. Lin, C.Y. Tsai, C.-C. Wang, Enhancement of thermal conductivity with cu for nanofluids using chemical reduction method, Int. J. Heat Mass Transfer 49 (2006) 3028–3033.
[27] J. Philip, P.D. Shima, B. Raj, Evidence for enhanced thermal conduction through percolating structures in nanofluids, Nanotechnology 19 (2008) 305706.
[28] J. Buongiorno, D.C. Venerus, N. Prabhat, T. McKrell, J. Townsend, R. Christianson, Y.V. Tolmachev, P. Keblinski, L.-W. Hu, J.L. Alvarado, I.C. Bang, S.W. Bishnoi, M. Bonetti, F. Botz, A. Cecere, Y. Chang, G. Chen, H. Chen, S.J. Chung, M.K. Chyu, S.K. Das, R. Di Paola, Y. Ding, F. Dubois, G. Dzido, J. Eapen, W. Escher, D. Funfschilling, Q. Galand, J. Gao, P.E. Gharagozloo, K.E. Goodson, J.G. Gutierrez, J. Hong, M. Horton, K.S. Hwang, C.S. Iorio, S.P. Jang, A.B. Jarzebski, Y. Jiang, L. Jin, S. Kabelac, A. Kamath, M.A. Kedzierski, L.G. Kieng, C. Kim, J.-H. Kim, S. Kim, S.J. Lee, K.C. Leong, I. Manna, B. Michel, R. Ni, J.E. Patel, J. Philip, D. Poulikakos, C. Reynaud, R. Savino, P.K. Singh, P. Song, T. Sundararajan, E. Timofeeva, T. Tritcak, A.N. Turanov, S. Van Vaerenbergh, D. Wen, S. Witharana, C. Yang, W.-H. Yeh, X.-Z. Zhao, S.-Q. Zhou, A benchmark study on the thermal conductivity of nanofluids, J. Appl. Phys. 106 (2009) 094312.
[29] K. Hong, T. Hong, H. Yang, Thermal conductivity of fe nanofluids depending on the cluster of nanoparticles, Appl. Phys. Lett. 88 (2006) 031901.
[30] N.R. Karthikeyan, J. Philip, B. Raj, Effect of clustering on the thermal conductivity of nanofluids, Mater. Chem. Phys. 109 (2008) 50–55.
[31] P.E. Gharagozloo, K.E. Goodson, J.K. Eaton, Impact of thermodiffusion on temperature fields in stationary nanofluids, in: Proceedings of ASME InterPACK, Vancouver, BC, 2007, p. 33293.
[32] S.D. Fortenberry, E.E. Dominguez-Ontiveros, D.R. Huitink, Y.A. Hassan, The temporal evolution of nanoparticle suspensions, Trans. Am. Nucl. Soc. 99 (2008) 785.
[33] P.E. Gharagozloo, J.K. Eaton, K.E. Goodson, Diffusion, aggregation, and the thermal conductivity of nanofluids, Appl. Phys. Lett. 93 (2008) 103110.
[34] R. Prasher, W. Evans, P. Meakin, J. Fish, P. Phelan, P. Keblinski, Effect of aggregation on thermal conduction in colloidal nanofluids, Appl. Phys. Lett. 89 (2006) 143119.
[35] R. Prasher, P. Phelan, P. Bhattacharya, Effect of aggregation kinetics on the thermal conductivity of nanoscale colloidal solutions (nanofluids), Nano Lett. 6 (2006) 1529–1534.
[36] J. Eapen, J. Li, S. Yip, Beyond the Maxwell limit: thermal conduction in nanofluids with percolating fluid structures, Phys. Rev. E 76 (2007) 062501.
[37] B. Wang, L. Zhou, X. Peng, A fractal model for predicting the effective thermal conductivity of liquid with suspension of nanoparticles, Int. J. Heat Mass Transfer 46 (2003) 2665–2672.
[38] J.A. Eastman, S.R. Phillpot, S.U.S. Choi, P. Keblinski, Thermal transport in nanofluids, Annu. Rev. Mater. Res. 34 (2004) 219–246.
[39] W. Evans, R. Prasher, J. Fish, P. Meakin, P. Phelan, P. Keblinski, Effect of aggregation and interfacial thermal resistance on thermal conductivity of nanocompsites and colloidal nanofluids, Int. J. Heat Mass Transfer 51 (2008) 1431–1438.
[40] P.E. Gharagozloo, K.E. Goodson, Aggregate fractal dimensions and thermal conduction in nanofluids, J. Appl. Phys. 108 (2010) 074309.
[41] J. Philip, P.D. Shima, R. Baldev, Nanofluid with tunable thermal properties, Appl. Phys. Lett. 92 (2008) 043108.
[42] J. Buongiorno, Convective transport in nanofluids, J. Heat Transfer 128 (2006) 240–250.
[43] D. Wen, Y. Ding, Effect of particle migration on heat transfer in suspensions of nanoparticles flowing through minichannels, Microfluid. Nanofluid. 1 (2005) 183–189.
[44] R. Savino, D. Paterna, Thermodiffusion in nanofluids under different gravity conditions, Phys. Fluids 20 (2008) 017101.
[45] T.A. Witten, L.M. Sander, Diffusion-limited aggregation, a kinetic critical phenomenon, Phys. Rev. Lett. 47 (1981) 1400–1403.
[46] P. Meakin, J.M. Deutch, Monte Carlo simulation of diffusion controlled colloid growth rates in two and three dimensions, J. Chem. Phys. 80 (1984) 2115–2122.
[47] L.A. Spielman, O. Levenspiel, A Monte Carlo treatment for reacting and coalescing dispersed phase systems, Chem. Eng. Sci. 20 (1965) 247–254.
[48] B.H. Shah, D. Ramkrishna, J.D. Borwanker, Simulation of particulate systems using the concept of the interval of quiescence, AIChE J. 23 (1977) 897–904.

[49] K. Liffman, A direct simulation Monte-Carlo method for cluster coagulation, J. Comput. Phys. 100 (1992) 116–127.
[50] F.E. Kruis, A. Maisels, H. Fissan, Direct simulation Monte Carlo method for particle coagulation and aggregation, AIChE J. 46 (2000) 1735–1742.
[51] N. Metropolis, S. Ulam, The Monte Carlo method, J. Am. Stat. Assoc. 44 (1949) 335–341.
[52] R. Jullien, R. Botet, Aggregation and Fractal Aggregates, World Scientific, 1987.
[53] M. Smoluchowski, Drei Vorträge über Diffusion brownsche Bewegung und Koagulation von Kolloidteilchen, Phys. Z. 17 (1916) 557–585.
[54] H.J. Pearson, I.A. Valioulis, E.J. List, Monte Carlo simulation of coagulation in discrete particle-size distributions. Part 1. Brownian motion and fluid shearing, J. Fluid Mech. 143 (1984) 367–385.
[55] R. Landauer, Electrical conductivity in inhomogeneous media, AIP Conf. Proc. 40 (1978) 2.
[56] C.-W. Nan, R. Birringer, D.R. Clarke, H. Gleiter, Effective thermal conductivity of particulate composites with interfacial thermal resistance, J. Appl. Phys. 81 (1997) 6692–6699.
[57] J.C. Maxwell, A Treatise on Electricity and Magnetism, second ed., Clarendon, Oxford, 1881. p. 365.
[58] A.A. Potanin, R. De Rooij, D. Van den Ende, J. Mellema, Microrheological modeling of weakly aggregated dispersions, J. Chem. Phys. 102 (1995) 5845–5853.
[59] S.R. de Groot, P. Mazur, Non-equilibrium Thermodynamics, Interscience Pub., New York, 1962. pp. 273–284.
[60] S.A. Putnam, D.G. Cahill, G.C.L. Wong, Temperature dependence of thermodiffusion in aqueous suspensions of charged nanoparticles, Langmuir 23 (2007) 9221–9228.
[61] R.J. Hunter, Foundations of Colloid Science, Oxford University Press, New York, 2001.
[62] L.H. Hanus, R.U. Hartzler, N.J. Wagner, Electrolyte-induced aggregation of acrylic latex. 1. Dilute particle concentrations, Langmuir 17 (2001) 3136–3147.
[63] W.N. Russel, D.A. Saville, W.R. Schowalter, Colloidal Dispersions, Cambridge University Press, Cambridge, UK, 1989.
[64] E.P. Honig, G.J. Roebersen, P.H. Wiersema, Effect of hydrodynamic interaction on the coagulation rate of hydrophobic colloids, J. Colloid Interf. Sci. 36 (1971) 97–109.
[65] E.J.W. Verwey, J.Th.G. Overbeek, Theory of the Stability of Lyophobic Colloids, Elsevier, Amsterdam, 1948.
[66] M. Schudel, S.H. Behrens, H. Holthoff, R. Kretzschmar, M. Borkovec, Absolute aggregation rate constants of hematite particles in aqueous suspensions: a comparison of two different surface morphologies, J. Colloid Interf. Sci. 196 (1997) 241–253.